Modelling and optimized water management of artificial inland waterway systems

J. Wagenpfeil, E. Arnold, H. Linke and O. Sawodny

ABSTRACT

A decision support system (DSS) for optimized operational water management of artificial inland waterways is presented. It will be deployed as part of a supervisory control and data acquisition (SCADA) system of the Mittellandkanal (MLK), a large canal structure in northern Germany, and relies on experience gained from a similar system. The DSS uses a model predictive controller with a 48 h prediction horizon to calculate optimal pump and discharge strategies that will ensure navigable water levels and at the same time minimize operational costs. The internal process model for the model predictive controller is obtained from a numerical integration of the Saint Venant equations using Godunov's method. The initial state needed for an accurate prediction is estimated using moving horizon state estimation (MHE) or unscented Kalman filtering. Additionally, the state estimation methods are used to estimate non-measurable disturbance inflows, which may have a strong impact on the control performance if not compensated for by the model predictive controller. The optimal control strategy is transformed into discrete-valued pump and discharge jobs that account for technical and operational input constraints. Closed-loop simulations with a high-resolution hydrodynamic numerical model of the MLK illustrate the ability of the control algorithm to adapt to model uncertainties and non-controllable inputs.

Key words | model predictive control, open-channel control, optimal control, Saint Venant equations, state estimation, water management

J. Wagenpfeil (corresponding author)
E. Arnold
O. Sawodny
Institute for System Dynamics,
University of Stuttgart,
P. O. Box 80 11 40,
D-70511 Stuttgart,
Germany
E-mail: *wagenpfeil@isys.uni-stuttgart.de*

H. Linke
Fraunhofer Institute of Optronics,
System Technology and Image Exploitation,
Application Center System Technology,
Am Vogelherd 50,
D-98693 Ilmenau,
Germany

INTRODUCTION

Open-channel hydraulic systems, such as irrigation channels, drainage canal systems, river reservoir cascades or inland waterways, are spatially distributed systems with dynamics that vary with the operating conditions. The main purpose of operational water management of inland transportation waterways is to ensure the safety and operability of navigation. Therefore, water levels must be maintained within narrow limits in order for the waterways to be navigable. This is particularly true for artificial waterways, which will be referred to as *canals*. Where a canal traverses a sloped area, it may be divided into several segments of different elevation called *reaches* or *sections*. Generally, reaches can be considered as self-contained water volumes of a water body that are connected by *locks* (typical for rivers and transportation canals), weirs (typical for rivers or irrigation canals) or similar separating structures.

A common problem of almost all canals is the water supply, since a certain amount of water is lost from the higher reach each time a ship goes through a lock. This water loss has to be compensated for. Drainage and evaporation during the dry season result in an additional loss of water. As most canals – unlike rivers – do not have a natural tributary, water has to be taken from nearby sources such as rivers or lakes. However, the amount of water that can be used to feed the canal may be, depending on the season, limited and in some cases, there may not even be a water supply available. To avoid a drop of the water level in the upper sections of the canal, water must be pumped up from lower reaches. Under some conditions, such as heavy rains or

doi: 10.2166/hydro.2012.163

flood, water levels might exceed the upper limits, and water has to be discharged from the canal. In particular situations, heavy wind stress may locally cause a violation of the bounds on the water levels, and a combined pump and discharge strategy may be necessary. An optimal water management strategy will compensate for water losses and other disturbances to maintain navigable water levels, even under difficult conditions and at the same time minimize operational costs.

In the following, a model predictive control (MPC)-based decision support system (DSS) for optimized water management of the canal system in the water management district Rothensee, Germany, is presented. This canal system consists of the eastern reach of the Mittellandkanal (MLK), the two reaches of the Elbe-Havel-Kanal (EHK) and the Rothenseer Verbindungskanal (RVK), which connects the port of Magdeburg with the MLK and the Elbe river, as shown in Figure 1. Under normal conditions, the natural water inflow into the canal system is insufficient to maintain the required water levels. Pump stations in Rothensee and Hohenwarthe are used to transport water from the RVK and Zerben section of the EHK into the eastern section of the MLK. Pump stations in Magdeburg and Niegripp are used to pump water from the Elbe into the RVK and the Zerben section of the EHK. Discharges are located near the eastern end of the MLK, and are used to discharge water from the MLK into the River Elbe.

The water management system presented in this paper extends a previously developed DSS for the water management of the Minden district, which governs the continuation of the canal system under consideration in the western direction, see Arnold *et al.* (1999a, b), Arnold & Linke (2002) and Linke (2005). The operational water management problem is formulated as an optimal control problem to minimize the energy costs caused by pump operations. For this purpose, the storage capacity of the canal system is utilized to shift the operational time of the pumps to low-cost periods of the electrical energy tariff. The state estimation process of the original DSS is extended to allow for the estimation of unknown, non-measurable additional inflows into the canal system. The estimated disturbance is used during the optimization to improve the robustness and overall control performance in the presence of large disturbances. The present paper is a revised version of preliminary results given in Wagenpfeil *et al.* (2010), extended by a comparative application of moving horizon state estimation (MHE) and unscented Kalman filtering for state and disturbance estimation. Additionally the robustness of the presented MPC algorithm against model uncertainties, especially concerning the bottom friction coefficients, is shown.

The basic concept of MPC is to use an internal dynamic model to predict the future behaviour of the system and obtain a control sequence that will achieve the desired control objective over a finite prediction horizon, see e.g. Rawlings & Mayne (2009). The first move of the optimal control sequence is applied, and after updating the internal model to the resulting new system state, a new optimal control sequence is computed. Regarding optimal water management, the optimal control sequence is the sequence of pump and discharge operations over the prediction horizon that minimizes the operational costs while maintaining navigable water levels. Hence, the control objective is formulated as

Figure 1 | (a) General map of the navigation canal system Mittellandkanal (MLK)/Elbe-Havel-Kanal (EHK) and (b) elevation of its sections.

an optimization problem with the cost function given by the operational costs and the state constraints given by the bounds on the water levels. The internal dynamic model used in this paper is based on a coarse-grid discretization of the Saint Venant equations. It provides a spatially dependent description of the state, unlike simplified methods such as the integrator delay (ID) model (see below). Using the internal dynamic model, a moving horizon state estimator, see e.g. Rawlings & Mayne (2009), determines the current system state based on level measurements taken over a finite past estimation time window.

There are several MPC applications for open-channel hydraulic systems reported in the literature. An incomplete overview will be given in the following. From a control engineering point of view, these approaches differ mainly in the type of internal prediction model (e.g. simplified dynamic models or approximations of the Saint Venant equations) and in the optimization objective (e.g. setpoint regulation or economic cost functions).

MPC is applied for water level and flow regulation in irrigation or drainage canal systems. In many cases, simplified dynamical models such as low-order linear discrete-time approximations are used as the internal process model of the model predictive controller, see e.g. Ruiz & Ramirez (1998) and Sawadogo *et al.* (1998). Taking the large-scale nature of irrigation canal systems into account, Negenborn *et al.* (2009) extend the MPC approach to a distributed control structure for serially connected subsystems. Kearney *et al.* (2011) integrate MPC into a hierarchical control structure. The upper MPC-based level generates control policies and accounts for load schedule predictions to provide optimal water-level reference trajectories for the low-level local PI-controllers of the canal reaches.

Parameter identification of simplified dynamic models is described, for example, by Wahlin (2004) for an ID model of a single reach from unsteady flow simulations of an irrigation canal system. Weyer (2001) describes low-order, linear and non-linear model derivations from system identification experiments on an irrigation channel.

Van Overloop (2006) describes an MPC application for a large drainage canal system. Internal models based on the discretized Saint Venant equations are compared with simple ID model approximations. A multiple model approach that uses several different models in parallel in the internal model accounts for uncertainties both in the model and in the inflows by suitable weighting of the different predictions in the MPC objective function. An implementation of a model predictive controller for operation of large pumping stations that accounts for a time-dependent energy demand is reported by Van Overloop *et al.* (2010).

MPC approaches are also applied for the control of river reservoirs, where additionally hydropower generation or flood protection must be taken into account. For example, Sohlberg & Sernfalt (2002) adapt grey box models for river control. Both the parameters and the state variables of the model are estimated by an extended Kalman filter (EKF). Thai (2005) approximates the Saint Venant equations by a system of ordinary differential equations using the method of lines. This model is used for non-linear MPC of a river reservoir system for flood protection. The state variables of the model are estimated from a stationary solution of the model equations. Likewise, a flood regulation problem is considered by Barjas Blanco *et al.* (2010). The authors approximate the hydrodynamic model by a simplified non-linear (conceptual) internal model of the MPC algorithm. Uncertainties of the rainfall predictions are included in the simulation to assess the robustness of the non-linear model predictive controller. Schwanenberg *et al.* (2011) describe parameter adaptation techniques for an internal prediction model based on the kinematic wave equations, which is applied in a non-linear MPC-based river network control scheme.

Ackermann *et al.* (2000) apply an MPC-based algorithm for maximization of hydropower generation and discharge wave attenuation of a river reservoir system. The internal model is a discretization of the simplified Saint Venant equations. The state variables of the model are estimated by an iterative procedure that identifies an additional inflow that minimizes the difference between model-based prediction and water-level measurement.

Hug-Glanzmann *et al.* (2005) linearize the Saint Venant equations around a stationary solution. The resulting linear partial differential equation system is discretized and then simplified by subsequent balanced model reduction. A Kalman filter is used to estimate the current values of the state variables from the water-level measurements. The supervisory controller for a cascade of river power plants is based on a model predictive approach. Due to the linear approximation, the open-loop optimal control problem can

be formulated as a constrained linear-quadratic optimal control problem that is efficiently solved by quadratic programming (QP) algorithms. In Setz *et al.* (2008), this approach is extended in two aspects: the discharge variations due to lock operations are included in the prediction model, and the restriction of the amount of applied control moves is considered by a hybrid model extension, which leads to a mixed-integer QP problem.

The control of the navigation canal system under consideration has to take into account the spatial distribution of the water due to pump or lock operations and wind stress. In contrast with many successful applications of simplified dynamic models for MPC of irrigation canal systems, a distributed parameter model is required here. The linearization of the Saint Venant equations as proposed by several authors is not appropriate for the canal system due to alternating water flow directions. For an optimal usage of the storage capacity, the whole canal system must be considered, and thus the minimum cost problem cannot be decomposed into decentralized sub-problems for each canal reach. The water management problem is therefore formulated as a large-scale non-linear optimization problem.

The remainder of this paper is organized as follows. At first, the internal dynamic model of the MPC algorithm is derived from the Saint Venant equations. Then, the open-loop optimal control problem is formulated. Subsequently, the observability problem and the state estimation procedures are discussed. Finally, simulation results of the closed-loop operation are given and the benefits of the optimal control approach are discussed.

UNSTEADY OPEN-CHANNEL FLOW

The internal process model of the model predictive controller has to describe the evolution of the water levels and flows with sufficient accuracy in space and time to reproduce short-term disturbances such as surge waves caused by lock operations and the influence of wind stress. At the same time, it must allow for a precise prediction of the long-term effects of lock operations and the water management strategy. A frequently used description for unsteady open-channel flow is given by the conservative form of the Saint Venant equations (see Appendix, available online at http://www.iwaponline.com/jh/015/163.pdf). The Saint Venant equations are derived from the mass and momentum balance, and form a set of quasi-linear hyperbolic partial differential equations. An analytical solution of these equations is generally not available and hence, there exist several approaches to simplify the Saint Venant equations.

One method is to linearize the Saint Venant equations around a stationary solution and under certain conditions, the resulting linear system may be solved analytically, see e.g. Baume *et al.* (1998). Alternatively, neglecting the inertia terms $Q_t + (Q^2/A)_\xi$ in the momentum equation of the Saint Venant equations results in the diffusive wave equation. By linearizing around a reference flow, the so-called Hayami equation is obtained, which can then be solved using Laplace transformation, see e.g. Litrico & Georges (1999). To apply either of these simplification methods, a stationary flow or at least a merely slowly varying flow must be assumed. While this is often true for systems with a natural gradient, for instance, rivers or irrigation channels, it generally does not hold for artificial waterways and particularly the canal system under consideration. Every reach of the canal system is characterized by relatively large varying flows in both directions of the stretch. Moreover, non-linear effects such as upsurges and downsurges caused by pump and lock operations can only be modelled by the full Saint Venant equations. This is supported by simulation results which show that the inertia terms in the momentum equation are of the same order of magnitude as the remaining terms and thus cannot be neglected.

Process model

To be used as the internal process model of the DSS, the full Saint Venant equations are numerically integrated using a first-order Godunov-type scheme. Such schemes exploit knowledge of the characteristic behaviour of the system and result in a full discretization of the system. Godunov-type schemes are mass conservative, which is important for a precise simulation of large bodies of standing water. Each reach of the canal system is first divided into n equidistant discrete cells whose area A and flow Q are assumed to be constant within each cell. The resulting piecewise constant distribution defines a sequence of Riemann problems at the discontinuities at the cell boundaries. The distribution of the states at the following discrete time step is obtained by piecing together the

solutions of these Riemann problems, using the approach developed by Roe (1981). This approach results in an explicit integration scheme, but delivers only an approximate solution of the Riemann problem, unlike implicit Riemann solvers, which are exact. The problem structure is, however, numerically beneficial, and the solution can be computed much more efficiently than with implicit schemes. Based on the frequency with which measurement data become available and to limit the computing time when solving the optimal control problem, a time step size of $\Delta t = 900$ s has been chosen. For a numerically stable simulation, the Courant–Friedrichs–Lewy condition requires that the spatial discretization step size $\Delta\xi$ satisfies:

$$\lambda_{\max}\Delta t \leq \Delta\xi \tag{1}$$

The maximum characteristic velocity $\lambda_{\max}$ gives an upper bound on the maximum propagation speed of any disturbance and can be approximated by:

$$\lambda_{\max} = v_{\max} + \sqrt{g h_{\max}} \tag{2}$$

where $v_{\max}$ is the maximum flow velocity and $h_{\max}$ the maximum water depth. Assuming no stationary flow $v_{\max}$ and a maximum water depth of 5 m also requires a minimal grid size of about $\Delta\xi = 6.5$ km for numerically stable integration. The resulting spatial resolution proves to be sufficient to model dynamical effects caused by pump or lock operations. A higher spatial resolution requires a better temporal resolution. This leads to a significantly increased computing time since the computational effort increases proportional to the fourth order of the spatial resolution. However, the improvement of the overall accuracy is small and does not justify the increased computational effort.

Consider a canal system with M reaches, where each discretized reach consists of n_i cells, $i = 1,\ldots, M$. Let $m = \sum n_i$ be the total number of cells of the canal system and let $\hat{k}$ be the current time step, then the resulting discrete-time process model for the whole canal system with 2 m states can be formulated as:

$$\mathbf{x}^{k+1} = \mathbf{f}^k\left(\mathbf{x}^k, \mathbf{u}^k, \mathbf{z}^k\right), \quad k \geq \hat{k} \tag{3}$$

with initial state $\mathbf{x}(\hat{k}) = \mathbf{x}_{\hat{k}}$ and $\mathbf{f}$ given by the numerical integration scheme. The state variables $\mathbf{x} = [\mathbf{x}_l\ \mathbf{x}_f]$ comprise the water levels $\mathbf{x}_l$ and flows $\mathbf{x}_f$ of the m discrete cells. Water levels are chosen as state variables instead of the wetted cross-sections due to the fact that most water management constraints are given as level constraints, as discussed later in this section. The notation $[\mathbf{x}\ \mathbf{y}]$ will be used in the following for the concatenation of the column vectors $\mathbf{x}$ and $\mathbf{y}$. The control variables:

$$\mathbf{u} = \begin{bmatrix}\mathbf{u}_p & \mathbf{u}_d\end{bmatrix} \tag{4}$$

are given by the pump flows $\mathbf{u}_p$ and discharge flows $\mathbf{u}_d$. Noncontrollable inputs, such as water demand of the locks $\mathbf{z}_l$, wind $\mathbf{z}_w$, and additional inflows $\mathbf{z}_f$, are expressed by:

$$\mathbf{z} = [\mathbf{z}_l \quad \mathbf{z}_w \quad \mathbf{z}_f] \tag{5}$$

Model parametrization

The simulation model is parametrized based on geometry data in the form of cross-sectional profiles that are measured every 100 m. The profiles were provided by the Federal Waterways Engineering and Research Institute. The geometry of each profile is first approximated by a trapezoid. After that, trapezoids belonging to the same discrete cell of the process model are averaged to determine the geometry of that cell. The resulting trapezoidal prism shape of each cell is lastly fitted to optimally match the level-volume ratio of the original geometry. This step is necessary due to the assumption of an even canal ground, which causes a discrepancy between the level and the volume of a cell that must be corrected for. Table 1 shows the main model parameters such as the length, the number of discrete cells, the bottom elevation, the mean bottom width, the mean wall inclination and the mean Manning friction value for

Table 1 | Length L and resulting number of discrete cells n as well as the bottom elevation h_0, mean bottom width $\bar{b}$, the mean wall inclination $\bar{w}$ of each reach and the mean Manning friction coefficient $\bar{\eta}$

Canal reach	L [km]	n	h_0 [m]	$\bar{b}$[m]	$\bar{w}$	$\bar{\eta}$
MLK-Eastern section	87.8	14	51.7	36.9	0.331	40
EHK-Zerben	19.9	3	33.3	39.1	0.334	40
EHK-Wusterwitz	31.0	5	28.1	35.4	0.340	40
RVK	8.5	1	35.9	59.7	0.482	–

each reach of the canal system. Note that the reach RVK consists only of a single cell and is thus modelled by a simple volume balance. The bed friction force is computed using the semi-empirical Manning equation. Analogous to the geometry data, the friction parameters η of the discrete cells are determined from the geometry data provided by the Federal Waterways Engineering and Research Institute. The coefficients $C_1 = 9.57 \times 10^{-7}$ and $C_2 = 1.17 \times 10^{-6}$ of the quadratic approach for the wind stress were estimated and validated during development of the DSS in Minden and are re-used for the DSS presented here.

The process model is validated by comparative simulations with a high-resolution hydrodynamic numerical model of the canal system. The simulator CasCade+ (Bleninger *et al.* 2007) is based on an implicit discretization of the Saint Venant equations using the Preissmann schema and a grid with high resolution ($\Delta\xi = 100$ m, $\Delta t = 60$ s). Figures 2 and 3 show the results of a simulation scenario using the daily repeating pump cycle shown in Figure 4. By using the pump stations at both ends of the MLK-Eastern section, a step-like excitation of the flow is created every 24 h. After 8 h, the pumps are turned off again, which creates again a step-like excitation of the system. From the figures, it can be seen that the coarse-grid process model behaves almost identical to the high-resolution reference

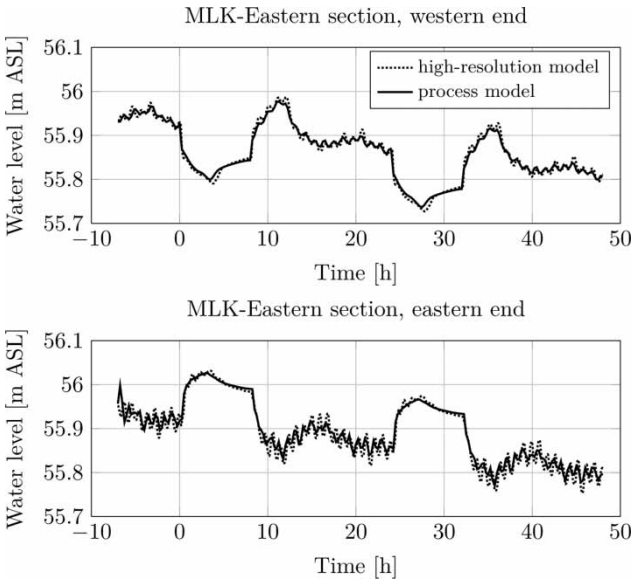

Figure 2 | Model comparison: water level (in metres above sea level (m ASL)) at both ends of the MLK-Eastern section.

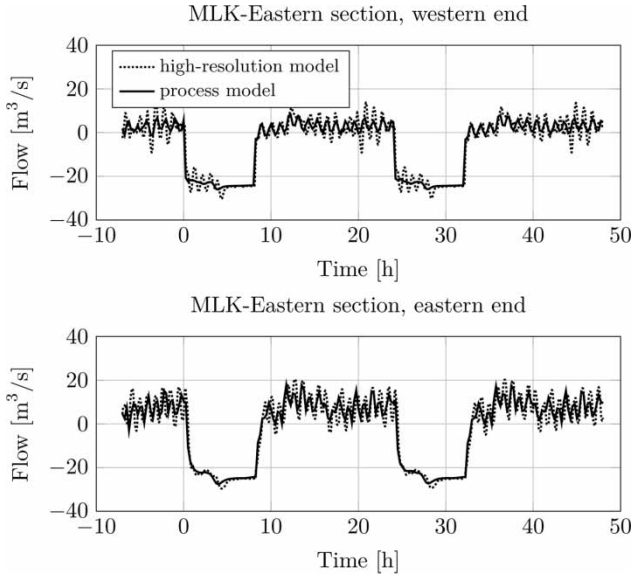

Figure 3 | Model comparison: flow at both ends of the MLK-Eastern section.

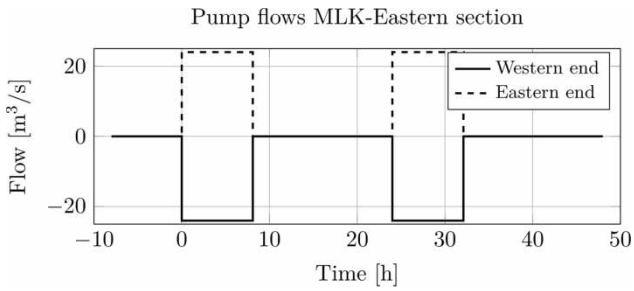

Figure 4 | Pump flows.

model for both the water levels and the flows. The process model sufficiently reproduces the static (e.g. water-level deviation under constant flow conditions, water level to water volume relation) and the dynamic (e.g. wave velocity, wave attenuation) behaviour of the high-resolution hydrodynamic numerical model. Between pump cycles, normal lock operations are simulated, which result in high-frequency waves that are damped to some extent by the process model due to the lower (spatial) resolution.

Table 2 shows the mean error and standard deviation between the simulated water levels and flows obtained with the coarse-grid process model and the high-resolution model.

The water levels are very well reproduced, with a standard deviation of only around 1 cm, and a negligible mean error. The mean error of the water flows is even smaller,

Table 2 | Simulation error of the process model (in relation to CasCade+) for each discrete cell of the reach MLK-Eastern section and the mean absolute error (MAE) across all cells

	Level [mm]		Flow [m³/s]	
	Mean	Std. dev.	Mean	Std. dev.
Cell 1	0.4	7.2	0.0	2.9
Cell 2	0.5	8.7	0.0	2.2
Cell 3	0.6	8.2	0.0	2.7
Cell 4	1.0	7.5	0.1	3.1
Cell 5	0.4	9.8	0.0	3.0
Cell 6	−0.3	9.9	0.0	3.1
Cell 7	−0.7	8.9	0.1	3.7
Cell 8	−1.0	9.4	0.0	3.5
Cell 9	−1.4	12.1	0.0	3.3
Cell 10	−1.4	11.4	0.0	4.1
Cell 11	−1.7	13.3	0.1	3.3
Cell 12	−2.1	10.0	0.0	4.0
Cell 13	−2.4	12.1	0.0	3.6
Cell 14	−3.2	9.8	0.1	6.5
MAE	1.2	9.9	0.0	3.5

and the comparably high standard deviation is mainly caused by the damping of high-frequency waves. The process model accurately simulates the long-term evolution of the system and shows only moderate damping of highly dynamic disturbances, which makes it suitable for use as internal process model of the model predictive controller.

MPC ALGORITHM

MPC, also known as receding horizon control, is an iterative control method that uses a process model to simulate the future evolution of the system state starting at the current step $\hat{k}$ over a finite prediction horizon $\mathcal{K}_{\text{opt}} = \left\{\hat{k},\ \ldots \hat{k}+K\right\}$, see Figure 5. Based on the process model, an optimal control sequence (u) is determined that minimizes a predefined objective function which mathematically models the desired process behaviour. The system behaviour (y) may be subject to constraints ($y_{\min}, y_{\max}$). To account for the finite optimization horizon and unmodelled disturbances, only the first step of the control sequence is applied. The prediction window is then shifted one step ahead in time and a new

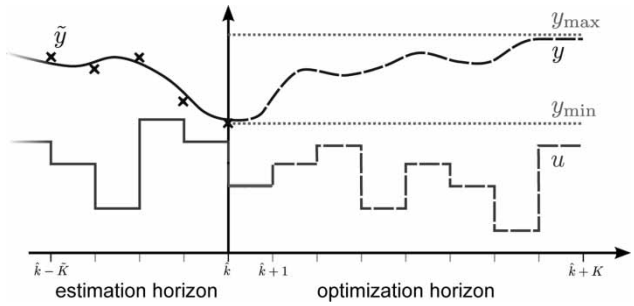

Figure 5 | Time horizons for model predictive control and moving horizon state estimation.

optimal control sequence is determined. Through the repeated computation and application of the control, the desired process behaviour is achieved.

The main goal of the canal water management is maintaining navigable water levels with minimal pump costs. Hence, the objective function of the optimal control problem takes the form:

$$J_1 = \sum_{k=\hat{k}}^{\hat{k}+K-1} \left[[\mathbf{c}_e^k(\mathbf{u}_p^k)]^T \mathbf{u}_p^k + \mathbf{c}_d^T \mathbf{u}_d^k + [\boldsymbol{\rho}_r(\mathbf{u}^k)]^T \mathbf{u}^k \right] \tag{6}$$

where $\mathbf{c}_{\text{e}}^k$ is the electrical energy cost on pump operations $\mathbf{u}_{\text{p}}$. The energy cost depends on the electrical work that is done by each pump and the electrical energy price. A particularity here is the fact that the electrical energy tariff does not depend on the time of day but on the total electrical power consumed. Up to a certain power level (1,800 kW), the electrical energy price is 0.09 €/kWh. Above this level, the energy price increases to 0.13 €/kWh. The coefficient $\mathbf{c}_{\text{d}}$ formulates a fictitious discharge cost that is used to minimize discharge operations $\mathbf{u}_{\text{d}}$ and chosen to be of the same order of magnitude as the average pump cost. The regularization cost $\boldsymbol{\rho}_{\text{r}}$ is a tuning parameter used to smooth the optimal control sequence. Its value is chosen such that the resulting penalty is of the same order of magnitude as the total pump cost.

One of the advantages of MPC is the fact that state and control constraints can be directly taken into account. Pump and discharge flow constraints are given as limits on the control variables in the form:

$$\mathbf{0} \leq \mathbf{u}^k \leq \mathbf{u}_{\max}^k \tag{7}$$

The requirement of navigable water levels results in bounds on the water levels $\mathbf{x}_{\mathrm{l}}$ in the form:

$$\begin{aligned} &\mathbf{x}_{l,\min} \le \mathbf{x}_l^k \le \mathbf{x}_{l,\max}, \\ &\mathbf{x}_{v,\min} \le \mathbf{g}_v(\mathbf{x}_l^k) \le \mathbf{x}_{v,\max}, \end{aligned} \tag{8}$$

with the lower and upper water levels $\mathbf{x}_{\mathrm{l},\min}$ and $\mathbf{x}_{\mathrm{l},\max}$, respectively, see Table 3. In addition, the water volumes of the reaches of the canal system $\mathbf{g}_{\mathrm{v}}(\mathbf{x}_{\mathrm{l}})$ are constrained in a similar fashion by the lower and upper limits $\mathbf{x}_{\mathrm{v},\min}$ and $\mathbf{x}_{\mathrm{v},\max}$, respectively. These bounds on the water volume of each reach can be interpreted as restrictions on the mean water level of the respective reach.

However, applying these bounds as hard constraints on the state variables may result in an infeasible optimization problem under some conditions, such as flooding or high wind stress. Therefore, the water level and volume restrictions (8) are transformed to soft constraints by introducing slack variables and adding a penalty term to the objective function, see e.g. Rao *et al.* (1998). The relaxed constraints on the water levels and volumes are then given by:

$$\begin{aligned} &\mathbf{x}_{l,\min} - \boldsymbol{\eta}_l^k \le \mathbf{x}_l^k \quad \le \mathbf{x}_{l,\max} + \boldsymbol{\eta}_l^k, \quad \boldsymbol{\eta}_l^k \ge \mathbf{0} \\ &\mathbf{x}_{v,\min} - \boldsymbol{\eta}_v^k \le \mathbf{g}_v(\mathbf{x}_l^k) \le \mathbf{x}_{v,\max} + \boldsymbol{\eta}_v^k, \quad \boldsymbol{\eta}_v^k \ge \mathbf{0} \end{aligned} \tag{9}$$

with the slack variables $\boldsymbol{\eta}_{\mathrm{l}}^k$ and $\boldsymbol{\eta}_{\mathrm{v}}^k$. These slack variables are included in the objective function as additional optimization variables with weights $\boldsymbol{\rho}_{\mathrm{l}}$ and $\boldsymbol{\rho}_{\mathrm{v}}$ to penalize a violation of the state constraints, and the resulting objective function is given by:

$$J = J_1 + \sum_{k=\hat{k}}^{\hat{k}+K} \left[\boldsymbol{\rho}_{\mathrm{l}}^T \boldsymbol{\eta}_{\mathrm{l}}^k + \boldsymbol{\rho}_{\mathrm{v}}^T \boldsymbol{\eta}_{\mathrm{v}}^k \right] \tag{10}$$

Table 3 | Water level and volume limits for the canal system

Canal reach	$\mathbf{x}_{\mathrm{l,min}}$ [m]	$\mathbf{x}_{\mathrm{l,max}}$ [m]	$\mathbf{x}_{\mathrm{v,min}}$ [10^6 m^3]	$\mathbf{x}_{\mathrm{v,max}}$ [10^6 m^3]
MLK-Eastern section	55.90	56.40	18.41	19.52
EHK-Zerben	37.35	37.65	4.19	4.58
EHK-Wusterwitz	32.15	32.50	5.91	6.57
RVK	39.60	39.80	2.16	2.29

The penalty weights $\boldsymbol{\rho}_{\mathrm{l,v}}$ are tuned such that the solution is admissible under normal conditions. The optimization horizon should cover the essential dynamics of the system. A period of 24 h was chosen as the basis for the optimization horizon to cover daily recurring operation schedules. However, an optimization horizon of only 24 h is not long enough to cover the typical behaviour of the whole canal system. Eventually, a value of 48 h ($K = 192$) was chosen for the optimization horizon, which is a compromise between the accuracy of the prediction and a far enough outlook to avoid shortsighted management suggestions. The long-term control performance is further improved by tuning the final time ($k = \hat{k} + K$) water volume constraints in Equation (9).

The optimization problem in every step $\hat{k}$ is then given by:

$$\min_{\substack{\mathbf{x}^k, \mathbf{u}^k, \boldsymbol{\eta}_{\mathrm{l}}^k, \boldsymbol{\eta}_{\mathrm{v}}^k \\ k=\hat{k},\ldots,\hat{k}+K}} J \tag{11}$$

subject to the system dynamics (3) and control and state constraints (7) and (9). It is solved as a large-scale structured non-linear programming problem in the state, control and slack variables by a sequential QP algorithm, using the software library HQP (Franke *et al.* 2012), which takes into account the structure of the cost function and constraints, especially the sparsity structure of the derivative matrices, see Arnold *et al.* (1997) for details. A typical problem size is approximately 4,000 variables, 3,000 equality and 8,000 inequality constraints. It takes about 16 s on an Intel Core 2 Duo running at 2.8 GHz to compute the optimal control sequence.

Predictions of non-controllable inputs

Predictions of non-controllable inputs, such as water demand of the locks $\mathbf{z}_{\mathrm{l}}$, wind $\mathbf{z}_{\mathrm{w}}$, and additional inflows $\mathbf{z}_{\mathrm{f}}$ are required for the optimization of the future system behaviour within the MPC algorithm. Two different algorithms for prediction of the lock operation and hence the water demand of the locks are developed and compared with operational data from the MLK/ESK canal system. The first algorithm takes into account the weekly

periodicity, and forecasts the lock operation to be identical to the equivalent time period 1 week before. The prediction proved to be susceptible to disturbances, such as holidays on weekdays, maintenance work at locks, or communication failure of the supervisory control and data acquisition (SCADA) system. An improved algorithm exploits long-term average values of lock operation under normal operating conditions resulting in a monthly classification for different categories of days (working days, Saturdays, Sundays/holidays). The average prediction error for a 3 month period, which was examined in detail, is in the range 9.2–28.9% for the different locks, which is an improvement over the first approach (between 12.9 and 35.6%). However, the maximum percental prognosis error remains large (250% compared with 267%), as, for particular situations with a very low number of realized lock operations (e.g. because of maintenance measures at the lock or traffic limitations for the canal), there is no special treatment available yet.

Forecasts of the wind direction and wind velocity $\mathbf{z}_w$ within the optimization horizon are obtained as online data from Germany's National Meteorological Service. There are only a few forecasts of additional inflows $\mathbf{z}_f$ into the canal system available. Therefore, the state estimation algorithm is extended for an estimation of a distributed disturbance inflow, see below. The estimated inflows are employed as inflow predictions.

Discrete-valued control inputs

A pump station consists of a number of pumps, where each pump can be either operated at a given constant flow rate or turned off. Hence the flow rate of a pump station is discrete valued and in the usual case of identical pumps for each single pump station the number of flow-rate levels is equal to the number of pumps plus zero flow. Additionally, there are constraints on the minimum operating time of each single pump, as well as on the minimum idle time between pump operations. The same applies to discharge stations. Therefore, the control variables of the optimal control problem (3)–(7) and (9)–(11) are discrete valued and thus it is a mixed-integer non-linear programming problem (MINLP). Unfortunately, there is no algorithm available that can solve an MINLP with several hundred or thousand variables with reasonable computational effort.

A two-stage method is therefore applied to calculate the optimal pump and discharge strategies: in the first stage, the optimal control problem (3)–(7) and (9)–(11) is solved for continuous-valued pump and discharge flows, i.e. the integrality constraints are relaxed. In the second stage, these continuous-valued trajectories are approximated by the number of operating pumps and discharges and their respective running time. The second stage is accomplished independently for each single device and is formulated in the following as an optimal control problem for a single station.

The control variable is the discrete-valued flow u_D^k that approximates the continuous valued flow u^k. The state variable x_I^k represents the integral of the difference between these flows and x_D^k the running time of the current pump or discharge configuration:

$$x_D^{k+1} = \begin{cases} x_D^k + \Delta t, & \text{if } u_D^k = u_D^{k-1}, \\ 0, & \text{otherwise,} \end{cases} \quad k = \hat{k}, \ldots, \hat{k} + K - 1$$
$$x_I^{k+1} = x_I^k + \left(u_D^k - u^k\right)\Delta t, \quad x_I^{\hat{k}} = 0 \tag{12}$$

Both the initial state $x_D^{\hat{k}}$ and $u_D^{\hat{k}-1}$ are given by the device operation in the previous time steps. The discrete-valued trajectory $\{u_D^k\}$ is obtained by minimization of the approximation error:

$$\min_{u_D^k,\, k=\hat{k},\ldots,\hat{k}+K-1} \left\{ \sum_{k=\hat{k}}^{\hat{k}+K-1} \alpha_P^k \left(u_D^k - u^k\right)^2 + \sum_{k=\hat{k}}^{\hat{k}+K} \alpha_I^k \left(x_I^k\right)^2 \right\} \tag{13}$$

taking into account the constraints:

$$\left.\begin{array}{ll} u_D^k \in \mathcal{U}_D & \text{if } x_D^k \geq T_{\min} \\ u_D^k = u_D^{k-1} & \text{otherwise} \end{array}\right\}, \quad k = \hat{k}, \ldots, \hat{k} + K - 1 \tag{14}$$

where $\mathcal{U}_D$ denotes the feasible discrete flow levels. For simplicity of notation, the minimum pump operating and idle time specifications are aggregated into a single minimum time interval $T_{\min}$ between flow-rate changes in Equation (14).

α_P and α_I are weighting coefficients for the proportional and the integral deviation of the discrete-valued flow from the continuous-valued flow, respectively. These parameters have to be adjusted to obtain a discrete-valued flow time series that tracks the solution of the continuous-valued optimal control problem.

A discrete dynamic programming algorithm is applied for solution of the discrete optimal control problem (12)–(14). Figure 6 shows exemplary the approximation results for a pump station with four pumps of 4 m^3/s each.

This two-stage method is similar to the sum-up rounding strategy described by Sager (2005). It guarantees an integer feasible solution while minimizing the deviation of the discrete-valued flow from the solution of the relaxed optimal control problem.

The resulting pump and discharge jobs are then checked and confirmed where appropriate by the operating staff of the process control station. The open-loop optimal control problem is repeated after 2 h with an accordingly shifted prediction horizon K_{opt} equivalent to eight discrete time steps. Therefore, not only the first, but the first eight steps of the computed optimal control sequence must be applied to the process. The decision to re-calculate the optimal control strategy only every 2 h has been taken to balance the desire for a quick response to changing operating conditions with a manageable workload for the staff.

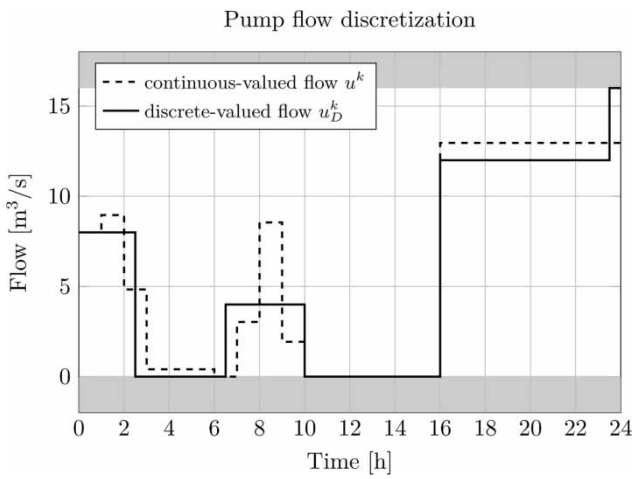

Figure 6 | Approximation of the continuous-valued pump flow u^k by the discrete-valued flow u_D^k.

STATE ESTIMATION

The MPC algorithm determines the optimal control sequence based on a prediction of the further evolution of the system states. For that, the current system state $x_{\hat{k}}$ at the beginning of the prediction horizon must be known, i.e. the current water level and flow in each discrete cell of the coarse-grid process model should be determined. Water-level gauges distributed along the canal system provide measurements of the water levels for a subset of the discrete cells of the coarse-grid process model, given by the actual position of the gauges, as shown in Figure 1. The water levels in the remaining cells are unknown and must be estimated, as well as the water flows in all of the cells since measurements of the flow are not available. Under certain circumstances, such as unexpected heavy rainfall or flood, large non-measurable lateral inflows into the canal system might occur. To compensate for that, a distributed lateral disturbance inflow $\mathbf{z}_f$ shall be estimated. Additionally, the state estimation algorithm should also compensate for the inevitable measurement noise.

The impact of a successful identification of the distributed lateral disturbance inflow has already been recognized in the development stage of the preceding DSS. Similar to the extended MHE algorithm described later in this section, one additional inflow parameter for each reach of the canal system was introduced. The inflow was considered to be constant over the spatial dimension and the whole estimation horizon, and was successfully estimated in simulation studies. However, the practical application led to strong variations of the estimated inflow (see Figure 7) and even estimation failures, which eventually prevented its utilization within the model predictive controller. Among the reasons for the difficulties might have been inaccuracies of the process model and insufficient filtering of the estimated inflow signal. The main issues were, however, timing and communication problems of the SCADA system and water-level measurement errors. For instance, pump jobs that were suggested by the DSS could sometimes not be executed due to technical problems of the respective pump station. Failed pump or discharge jobs were, however, not reported back to the SCADA and thus unknown to

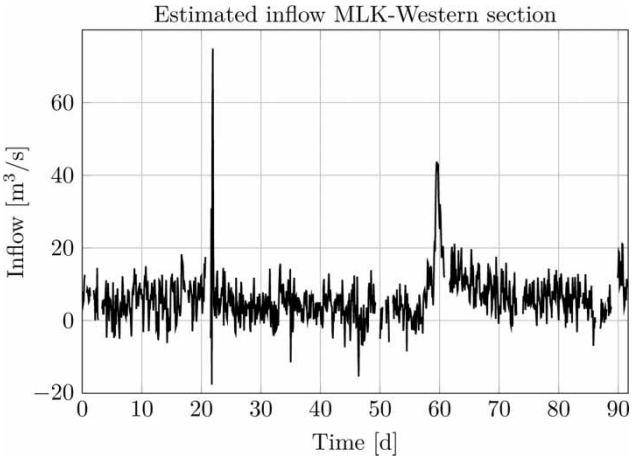

Figure 7 | Offline estimation of the inflow into the western reach of the MLK between 01 August 2007 and 31 October 2007, see Linke (2007). The gaps indicate failures of the state estimation procedure due to insufficient or erroneous measurements.

the state estimation algorithm. Those failed jobs were then mistaken as disturbance inflows by the MHE algorithm and caused a deterioration of the control performance. These issues will be mitigated to some extent, as the new SCADA system will provide more information about implemented and failed pump jobs. A key aspect of the development of the extended state estimation algorithm for this DSS is the tuning of the estimation-related parameters, like the estimation horizon, and improved filtering of the measurement data to reduce the impact of measurement errors.

Two different methods are employed for state observation, namely MHE and unscented Kalman filtering. MHE determines the state at the current time $\hat{k}$ from a least-squares problem that uses the process model and the available output measurements over a given estimation window. Using the known input over the estimation window, the moving horizon state estimator will determine the state at the beginning of the estimation window such that a forward simulation until $k = \hat{k}$ yields a minimum error between the simulated and the real measurements. Unscented Kalman filtering uses an iterative two-step algorithm that, during each time step, updates the previously estimated state by predicting the system evolution in a first step and correcting this prediction using the latest measurements in a second step. It uses the so-called unscented transformation to account for process noise during the prediction and measurement noise during the correction step. Assuming that the noise has a zero-mean normal distribution, then the unscented Kalman filter (UKF) will achieve a third-order approximation of the optimal state estimate regarding the mean square error.

Process model with noise

Let $\hat{k}$ be the current time step, then for each past time step $k < \hat{k}$ the process model used for state estimation can be formulated as:

$$\begin{aligned} \mathbf{x}^{k+1} &= \overline{\mathbf{f}}^{k}\left(\mathbf{x}^{k}, \overline{\mathbf{u}}^{k}, \mathbf{z}_{\mathrm{f}}^{k}\right) + \mathbf{v}_{\mathrm{p},x}^{k} \\ \mathbf{z}_{\mathrm{f}}^{k+1} &= \mathbf{z}_{\mathrm{f}}^{k} + \mathbf{v}_{\mathrm{p},z}^{k} \end{aligned} \tag{15}$$

where $\mathbf{v}_{\mathrm{p}}^{k} = [\mathbf{v}_{\mathrm{p},x}^{k} \quad \mathbf{v}_{\mathrm{p},z}^{k}]$ denotes additive process noise, and $\bar{\mathbf{u}}^{k} = [\mathbf{u}^{k} \quad \mathbf{z}_{\mathrm{l}}^{k} \quad \mathbf{z}_{\mathrm{w}}^{k}]$ the known past input given by the controllable inflows $\mathbf{u}^{k}$, the inflows caused by past lock operations $\mathbf{z}_{\mathrm{l}}^{k}$, and the wind stress $\mathbf{z}_{\mathrm{w}}^{k}$. The system is augmented with the unknown disturbance inflow $\mathbf{z}_{\mathrm{f}}$, which is assumed to be constant but affected by process noise. The model output $\mathbf{y}^{k} \in \mathbb{R}^{m}$ is given by:

$$\mathbf{y}^{k} = \mathbf{h}^{k}(\mathbf{x}^{k}) + \mathbf{v}_{\mathrm{m}}^{k} \tag{16}$$

where $\mathbf{h}^{k}$ is the measurement function and $\mathbf{v}_{\mathrm{m}}^{k}$ is additive measurement noise. Both the process and the measurement noise are assumed to be independent zero-mean normal distributed random variables.

Moving horizon state estimation

MHE transforms the observation problem into an optimization problem. Let $\hat{k}$ be the current time step, and let $\mathcal{K}_{\mathrm{est}} = \{\hat{k} - \tilde{K}, \ldots, \hat{k}\}$ be the estimation window. The idea behind MHE is to find initial states $\mathbf{x}^{\hat{k}-\tilde{K}}$ and $\mathbf{z}_{\mathrm{f}}^{\hat{k}-\tilde{K}}$ such that the simulated output $\mathbf{h}^{k}(\mathbf{x}^{k})$ optimally matches the real measured output $\tilde{\mathbf{y}}^{k}$ over the estimation window, see Figure 5.

Therefore, a weighted-norm objective:

$$J_{\mathrm{MHE}} = \Gamma\left(\mathbf{x}^{\hat{k}-\tilde{K}}, \mathbf{z}_{\mathrm{f}}^{\hat{k}-\tilde{K}}\right) + \sum_{k=\hat{k}-\tilde{K}}^{\hat{k}} \left(||\mathbf{v}_{\mathrm{p},x}^{k}||_{\mathbf{Q}_x}^2 + ||\mathbf{v}_{\mathrm{p},z}^{k}||_{\mathbf{Q}_z}^2 + ||\mathbf{v}_{\mathrm{m}}^{k}||_{\mathbf{Q}_m}^2\right) \tag{17}$$

with suitable weighting matrices $\mathbf{Q}_x$, $\mathbf{Q}_z$, and $\mathbf{Q}_m$, related to the noise covariance matrices is to be minimized:

$$\min_{\substack{\mathbf{x}^k,\mathbf{z}^k,\mathbf{v}_{\mathrm{p},x}^k,\mathbf{v}_{\mathrm{p},z}^k,\mathbf{v}_{\mathrm{m}}^k \\ \hat{k}-\tilde{K},\ldots,\hat{k}}} J_{\mathrm{MHE}} \tag{18}$$

subject to the extended process model (15) and taking into account the admissible ranges $\mathbf{x}^k \in \mathcal{X}$, $\mathbf{z}^k \in \mathcal{Z}$. The term Γ approximates the arrival cost, which summarizes the effects of past information before $\hat{k} - \tilde{K}$.

Due to a lack of data about the process noise of the canal model, $\mathbf{v}_{\mathrm{p},x}^k$ and $\mathbf{v}_{\mathrm{p},z}^k$ are neglected by setting the corresponding weighting matrices $\mathbf{Q}_x$ and $\mathbf{Q}_z$ to zero. The arrival cost Γ is approximated by a suitable (long) estimation horizon $\mathcal{K}_{\mathrm{est}}$. All model outputs $\mathbf{y}^k$ are water-level measurements with equal measurement noise. Therefore, the weighting matrix $\mathbf{Q}_m$ can be chosen as an identity matrix. The simplified MHE least-squares problem can be formulated as:

$$\min_{\substack{\mathbf{x}^{\hat{k}-\tilde{K}} \\ \mathbf{z}_{\mathrm{f}}^{\hat{k}-\tilde{K}}}} \sum_{k=\hat{k}-\tilde{K}}^{\hat{k}} \left|\left|\mathbf{h}^k\left(\mathbf{x}^k\right) - \tilde{\mathbf{y}}^k\right|\right|^2 \tag{19}$$

subject to the system dynamics (15) and the admissible ranges. From the solution of this problem, the current state $\mathbf{x}^{\hat{k}}$ and estimated inflow $\mathbf{z}_{\mathrm{f}}^{\hat{k}}$ are computed by subsequent forward simulation.

The MHE optimization problem (19) is non-linear and non-convex, however, its structure is very similar to the MPC problem and therefore the same numerical solution technique can be used. Moreover, since all past interconnecting flows, i.e. the lock, pump and discharge flows, are assumed to be known, the individual reaches can be decoupled for state estimation, which further simplifies the estimation problem compared with the optimal control problem.

Unscented Kalman filtering

The UKF was originally presented by Julier & Uhlmann (1997) as an alternative to the EKF. Given a stochastical dynamical system whose state can be considered as a normal-distributed random variable described by its mean and covariance, Kalman filtering provides recursive state estimates based on incomplete, noisy measurements. Each recursion consists of two steps: first, an *a priori* prediction of the mean and covariance of the state is calculated using the system dynamics and the previous estimate. In the second step, that prediction is updated, using the latest measurement to calculate the *a posteriori* estimate of the mean and covariance of the system state. For an optimal prediction with respect to the minimum mean squared error, the mean and covariance of the system state must be correctly captured while it is propagated through the system dynamics. In the case of linear systems, this is achieved by updating the estimated mean according to the system dynamics and transforming the estimated state covariance matrix with the state matrix. The EKF approximates the prediction of the new mean and covariance of the system state by propagating the mean through the non-linear system and transforming the covariance matrix using a linearization of the system equations. Depending on the type of non-linearity, this may introduce large errors between the estimated and true mean and covariance, which reduces the quality of the estimation and could even destabilize the filter.

The UKF uses the unscented transformation to calculate a more precise prediction of the mean and covariance of the state, and thus deliver an improved performance over the EKF. The unscented transformation is a deterministic sampling approach to capture the statistics of a random variable that is propagated through a non-linear function, i.e. the non-linear system dynamics in the case of the UKF. For a detailed description of how the unscented transformation is used to calculate the estimated state and disturbance inflow, please refer to the appendix (http://www.iwaponline.com/jh/015/163.pdf). In comparison to the more common extended Kalman filtering, unscented Kalman filtering has been shown to produce better results in many examples, e.g. Julier & Uhlmann (1997) and van der Merwe & Wan (2001). The fact that no derivatives are necessary is another great advantage regarding implementation in the case of

complex systems such as the canal system under consideration. The computational complexity of the UKF is similar to the EKF, particularly when using the square-root implementation of the UKF (UKF-SR) introduced by van der Merwe & Wan (2001). The computationally most complex part of the UKF is the calculation of the new sigma points, which requires the calculation of the matrix square root of the covariance matrix $\mathbf{P}$. While computing the square root using a Cholesky factorization $\mathbf{S}$ such that $\mathbf{S}\mathbf{S}^{\mathrm{T}} = \mathbf{P}$ is generally of complexity $\mathcal{O}(N^3/6)$, the UKF-SR implementation can be reduced to a complexity of $\mathcal{O}(N^2)$ by directly propagating the square root $\mathbf{S}$ between the iterations of the UKF-SR. More importantly, the numerical properties of the UKF-SR significantly improve compared with the normal UKF, which is rather prone to numerical problems concerning the definiteness of the covariance matrix $\mathbf{P}$. Due to these advantages, the UKF-SR is used for the simulation experiments presented later in this work.

Plausibility of state estimates

An important question regarding state estimation is whether the estimated state converges to the actual state, a problem closely connected to the observability of the dynamical system. For the partial differential equation system under consideration, a reasonable approach might be given by testing the discretized system (3) for observability. Due to the non-linearity of the system, this becomes computationally challenging for even very few discrete cells and is not feasible for the canal system under consideration.

Therefore, a different approach to verify the plausibility of the estimated states was chosen. After MHE, the discrete system is linearized along the trajectory of the estimated states. Then, for each step of the estimation window, observability of the linearized system is tested. By augmenting the system with the disturbance model, the estimated additional inflows are automatically included in the test for observability. Although (non-)observability of the linearized system gives no evidence on the observability of the non-linear system, simulation results indicate that observability of the states of a reach and one additional input is given if there is at least one measurement gauge that can be arbitrarily placed. Additionally, the estimated system output is compared with the measured output, and approximations of the confidence intervals for the estimated initial states are computed. The quality of the estimated states with respect to measurement noise is assessed by comparison of these confidence intervals with predefined threshold values. This is particularly helpful to identify circumstances when the estimation fails due to unanticipated disturbances, such as extreme non-measurable inflows or malfunctioning level gauges that provide flawed measurement data. The threshold values are to be tuned on qualified measurement data sets.

State estimation using unscented Kalman filtering gives an estimation of the current state as well as an estimation of the covariance of the states. These can similarly be used to verify the plausibility of the state estimates, as diverging covariances usually indicate problems during state estimation. It appears that the procedures taken are sufficient to verify the estimated state and indicate problems when state estimation might have failed.

SIMULATION RESULTS

The closed-loop behaviour of the MPC algorithm and the moving horizon state estimator is studied using the high-resolution model described before as a replacement for the real canal system. Lock operations are predicted based on long-term statistics. All unknown disturbance inflows into the MLK-Eastern section are combined to a single lateral disturbance inflow z_{f}, which is uniformly distributed over the whole length of the reach. Disturbance inflows into the remaining reaches are neglected. In the first simulation experiment, the closed-loop behaviour is simulated over 24 days with exact predictions of the non-controllable inputs, zero disturbance inflow z_{f}, and without wind stress. The dotted line in Figure 8 shows the simulated water level evolution at a representative level gauge near the western end of the MLK-Eastern section. Starting from steady-state conditions, the water level decreases and is kept just above its lower bound of 55.9 m (indicated by the grey area in Figure 8). The decreasing water level is caused by water loss of the reach due to lock operations, which must be compensated for by pump operations. Since this incurs electrical energy costs, the model predictive controller minimizes pumping, and the water level remains close to the lower limit. The water volume of the reach is equivalent to the

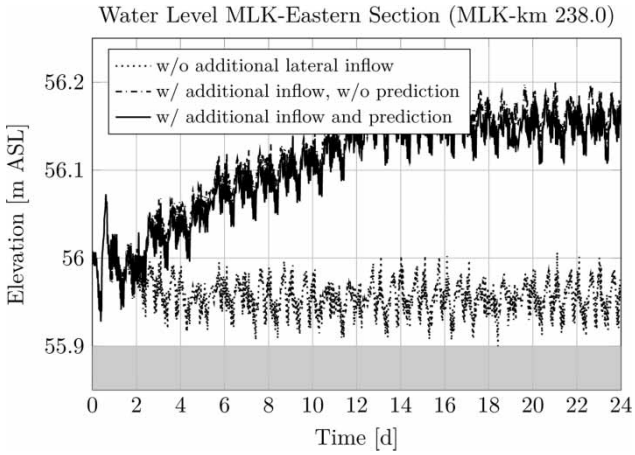

Figure 8 | Water level near the western end of the MLK-Eastern section. w/, with; w/o, without.

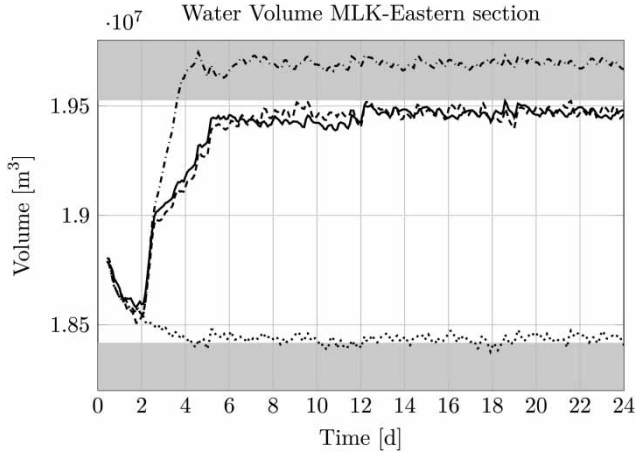

Figure 9 | Water volume in the MLK-Eastern section. Dotted line is 'w/o additional lateral inflow'; dash-dotted line is 'w/ additional inflow'; solid line is 'w/additional inflow and prediction'; dashed line is 'w/ additional inflow and prediction, model errors'.

mean water level and behaves accordingly, see Figure 9 (dotted line).

In the second simulation experiment, a constant additional inflow z_f of 11 m^3/s is applied in the simulation model, but not included in the prediction for the open-loop optimal control problem. Since this inflow is greater than the water loss due to lock operations (5.3 m^3/s), the water level increases, see the dash-dotted lines in Figures 8 and 9. After approximately 2 days, the upper volume bound (indicated by the grey area in Figure 9) is reached and kept by suitable discharge operations. Note the slight violation of the upper volume bound, which is a result of the disturbance flow. As mentioned in the MPC section, the hard constraints (8) are relaxed. Therefore, the optimal control problem remains feasible under these conditions, and the solution minimizes the predicted constraint violation.

In the third simulation experiment, the constant additional inflow z_f is estimated by the moving horizon state estimator and included in the prediction for the open-loop optimal control problem. The simulation results are similar to the second experiment, see solid lines in Figures 8 and 9, but the upper volume bound is not violated in this case due to the proper inflow prediction. Non-necessary pump and discharge operations are avoided, and the pump flow into the canal reach is reduced by approximately 4%.

Due to the fact that, so far, no real measurement data could be used to validate the parameterization of the process model, a fourth simulation experiment was performed with altered Manning friction coefficients. The canal model is relatively sensitive to variations of the bottom friction. Additionally, the friction coefficients cannot be measured (unlike the canal geometry, which is fairly precisely known), and therefore only rough estimates are available. To investigate the influence of the friction coefficients, the Manning value was increased from the nominal value used by the high-resolution model by about 42% to $\tilde{\eta} \approx 56.6\,m^{1/3}\,s^{-1}$. Although the open-loop model behaviour deviates considerably from the nominal behaviour, the closed-loop results (shown as the dashed line in Figure 8) are virtually identical to the previous simulation using the nominal friction parameters. The additional inflow is precisely estimated and compensated for by the model predictive controller, such that the water volume is kept right below the upper limit.

The quality of state and disturbance estimation is studied in further simulation experiments, focusing on the largest reach of the canal system, i.e. the eastern section of the MLK with a length of 88 km. The discretization process results in 14 discrete cells, where for six of those cells, water-level measurements are available. Consequently, the water levels of the remaining eight discrete cells and the water flow in all 14 cells must be estimated based on those measurements. In simulations without measurement noise, reasonable state estimations can be obtained using MHE with an estimation horizon of $\tilde{K} = 10$ time steps, corresponding to 2.5 h. A lateral disturbance inflow, simulated by a concentrated inflow (solid line in Figure 10) located 20 km off the western end is reliably estimated after increasing the estimation horizon to $\tilde{K} = 50$ time steps, corresponding to 12.5 h.

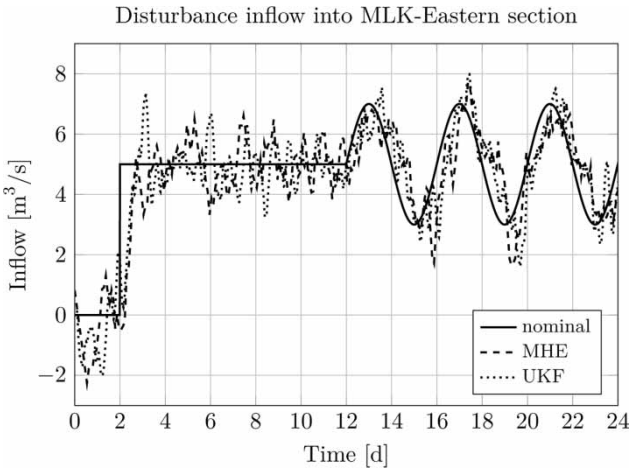

Figure 10 | Nominal and estimated disturbance inflow into the MLK-Eastern section.

Measurement noise is simulated by adding a zero-mean white noise signal with variance 0.01 m^2 to the water levels taken every simulated 60 s from the high-resolution model. As the internal process model of the MPC/MHE runs with a step size of 900 s, 15 measurement samples are averaged, such that the resulting standard deviation of the 900 s measurements is 0.025 m, a value that corresponds well to the actual standard deviation of the level measurements, which is between 0.01 and 0.03 m. This measurement noise results in strong noise on the estimated inflow, which must be compensated by further increasing the estimation horizon to $\tilde{K} = 84$ (21 h) to allow a reliable estimation of the additional inflow (dashed line in Figure 10). Increasing the estimation horizon has a similar effect as a low-pass filter by smoothing the estimated inflow as well as introducing a notable phase shift between the estimated and the nominal disturbance inflow.

For comparison, the UKF is fed with the same noisy data as the moving horizon state estimator for state and disturbance estimation. The parameters of the UKF are set to $\alpha = 10^{-3}$ and $\beta = 2$, and like the moving horizon state estimator, every 900 s, a new estimate is calculated. The process noise is assumed to be zero-mean and normal distributed, with a standard deviation of 0.02 m for the levels, 1 m^3/s for the flows and 0.2 m^3/s for the estimated inflow. The measurement noise is assumed to be zero-mean and normal distributed with a standard deviation of 0.1 m, which is more than the actual standard deviation of the measurement noise. Simulation experiments suggest that moderately overestimating the measurement noise results in a slightly better state estimation performance regarding the water levels and flows. The estimated inflow is additionally filtered using a first-order Butterworth low-pass filter with $10^{-5}\,s^{-1}$ cut-off frequency. The estimation of the disturbance inflow (dotted line in Figure 10) is very similar to the estimation obtained with MHE, following the nominal disturbance with a short delay and a considerable amount of noise. Likewise, the distribution of the inflow estimation errors of MHE and the UKF in Figure 11 are virtually the same, both with a standard deviation around 1 m^3/s. A more detailed evaluation of the mean estimation error and the standard deviation with respect to the state of every cell and the mean absolute error across all cells shows a similar result, slightly favouring the UKF, having a smaller mean estimation error regarding both water levels and flows (see Table 4). If the data are compared with Table 2, then it can be seen that the state estimation errors are close to the simulation error, with the exception of the estimated water flow, which seems to be slightly harder to estimate correctly.

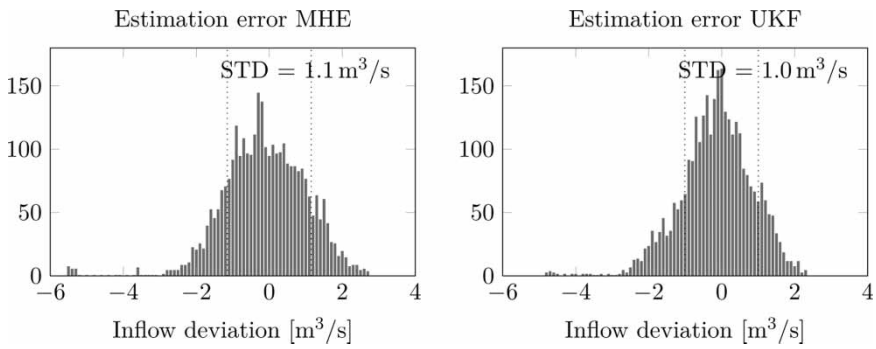

Figure 11 | Distribution and standard deviation (STD) of the estimation error.

Table 4 | Comparison between moving horizon state estimation and unscented Kalman filtering of the state estimation error for each discrete cell of the reach MLK-Eastern section and the mean absolute error (MAE) across all cells. Level measurements are available for discrete cells marked with*

	Level [mm]				Flow [m^3/s]			
	Mean		Std. dev.		Mean		Std. dev.	
	MHE	UKF	MHE	UKF	MHE	UKF	MHE	UKF
Cell 1*	1.8	1.3	11.1	8.6	−0.8	0.3	3.4	2.8
Cell 2*	2.4	1.0	13.1	9.0	−1.3	0.3	3.8	2.5
Cell 3	3.0	0.6	11.1	8.6	−0.9	0.6	4.7	3.0
Cell 4*	2.2	−0.0	13.2	8.0	1.4	0.9	4.2	3.3
Cell 5	−1.8	−0.6	13.2	9.2	3.6	1.2	3.6	3.2
Cell 6	−2.9	−1.3	11.8	9.4	0.7	−1.7	2.9	3.3
Cell 7	−0.1	−1.2	9.7	9.0	−2.1	−2.9	2.7	3.5
Cell 8*	4.2	−1.2	9.4	9.1	−3.8	−2.5	2.9	3.3
Cell 9	5.4	−1.1	10.7	11.8	−3.9	−2.1	3.5	3.3
Cell 10	7.1	−1.2	11.2	9.7	−3.1	−1.7	4.7	4.1
Cell 11*	4.8	−1.0	13.5	12.5	−1.1	−1.4	4.1	3.6
Cell 12	−2.8	−1.2	11.9	12.5	2.4	−1.0	4.0	4.0
Cell 13	−6.8	−1.3	15.5	13.3	3.7	−0.6	5.1	3.9
Cell 14*	3.7	−1.0	13.0	10.9	0.2	0.5	5.4	5.5
MAE	3.5	1.0	12.0	10.1	2.1	1.2	3.9	3.5

However, the performance of the state observation methods is sufficient for reliable estimates of the current state and appears to be mainly limited by the precision of the process model, especially in the case of the UKF.

Unscented Kalman filtering is an iterative algorithm that re-uses the latest state estimate, therefore the computation of the next iteration is comparably fast and takes about 0.1 s on an Intel Core 2 Duo running at 2.5 GHz. By contrast, MHE discards old state estimates and has to work an a comparably long estimation horizon, computing a new state estimate thus takes longer, approximately 5 s on the same machine. Considering that the DSS has to calculate a new proposition only every 2 h, the difference in calculating the time between the two state estimation methods can be neglected.

CONCLUSIONS

In this paper, an MPC-based DSS for optimized water management of artificial inland waterways is presented and applied to a large canal system in northern Germany. It extends a previously developed DSS for the western extension of the canal system under consideration, which has been reliably operating for over a decade. The internal process model of the model predictive controller is obtained from a numerical integration of the Saint Venant equations using a Godunov-type scheme and used to predict the water levels and flows of the canal reaches. The operational objectives, i.e. ensuring navigable water levels and minimizing electrical energy costs, led to a large-scale non-linear MPC open-loop optimal control problem. The MPC optimization problem is numerically solved at each time step to obtain the optimal control sequence. The optimal control sequence is transformed into a sequence of discrete-valued control inputs corresponding to pump and discharge job propositions. These take into account operational constraints for pump stations and discharges. The current system state at the beginning of the prediction horizon is determined using MHE, based on water-level measurements taken at several points along the canal system. Unscented Kalman filtering is introduced as an alternative state observation method. Based on operational experience gained with the original DSS, the state observation is extended to estimate a distributed disturbance inflow that summarizes all unknown inflows for each reach of the canal system.

Closed-loop simulations with a high-resolution model of the canal system under consideration show that the MPC algorithm provides excellent control performance. The pump and discharge jobs suggested by the DSS reliably keep the water levels within the boundaries of navigability. The MPC reliably compensates for errors and parameter uncertainties in the process model. Both state observation methods show an excellent quality of the estimated states. The UKF results in a slightly better performance than MHE with regard to the estimation error of state estimates and the estimated disturbance inflow. Although of no importance for the DSS described here, the computing time for the UKF is notably lower compared with MHE. The disturbance inflow is successfully estimated by both MHE and unscented Kalman filtering, and results in superior control performance when fed to the model predictive controller, but needs considerable smoothing in order to be used by the model predictive controller. Therefore, only slowly

changing disturbances, such as larger flood events or evaporation during dry periods, can be estimated with this method.

The DSS presented here will be integrated into the process control system SCADA of the canal system. The optimized pump and discharge jobs are presented to the operator of the process control system who must eventually decide whether to implement the proposed strategy or discard it based on experience. Completion of construction of an essential pump station and the following integration of the DSS into the SCADA system are scheduled for spring 2013, and tests are planned to begin soon afterwards. An important step of these tests will be the calibration of the process model with measured data, which has not been available so far. After successful implementation of the water management system, future plans envisage a cooperative process control that allows for a coordinated water management strategy together with the process control of the western extension of the canal system.

ACKNOWLEDGEMENTS

The authors gratefully acknowledge the Federal Waterways Engineering and Research Institute for providing the high-resolution simulation model and data of the canal system, as well as financial support of the project. The authors are also grateful to the anonymous reviewers whose valuable feedback helped to improve the quality of this paper.

REFERENCES

Ackermann, T., Loucks, D. P., Schwanenberg, D. & Detering, M. 2000 Real-time modeling for navigation and hydropower in the river Mosel. *Journal of Water Resources Planning and Management* **126** (5), 298–303.

Arnold, E. & Linke, H. 2002 Nonlinear model-predictive control of water level and flow for waterways. SIAM 50th Anniversary and 2002 Annual Meeting, Philadelphia, PA.

Arnold, E., Linke, H. & Franke, R. 1997 Optimal control application for operational water management of a canal system. 16th International Symposium on Mathematical Programming, Lausanne.

Arnold, E., Linke, H. & Puta, H. 1999a Nonlinear model predictive control for operational management of a canal system. *European Control Conference ECC'99*, Karlsruhe.

Arnold, E., Linke, H. & Puta, H. 1999b Optimal control application for operational water management of a canal system. *Studies in Automation and Information Technology* **24**, 7–16.

Barjas Blanco, T., Willems, P., Chiang, P.-K., Haverbeke, N., Berlamont, J. & De Moor, B. 2010 Flood regulation using nonlinear model predictive control. *Control Engineering Practice* **18** (10), 1147–1157.

Baume, J.-P., Sau, J. & Malaterre, P.-O. 1998 Modeling of irrigation channel dynamics for controller design. *IEEE Int. Conference on Systems, Man & Cybernetics (SMC'98)*, San Diego, CA, pp. 3856–3861.

Bleninger, T., Fenton, J. D. & Jirka, G. H. 2007 *Verfahrensbeschreibung des 1-D hydronumerischen Modellsystems CasCade+*. Tech. rep. 823. Institute for Hydromechanics, University of Karlsruhe, Karlsruhe, Germany.

Franke, R., Arnold, E. & Linke, H. 2012 HQP: a solver for sparse nonlinear optimization. URL: http://hqp.sourceforge.net.

Hug-Glanzmann, G., von Siebenthal, M., Geyer, T., Papafotiou, G. & Morari, M. 2005 Supervisory water level control for cascaded river power plants. *Hydropower Conference 05*, Stavanger.

Julier, S. J. & Uhlmann, J. K. 1997 A new extension of the Kalman filter to nonlinear systems. *11th Annual International Symposium Aerospace/Defense Sensing Simulation and Controls*, Orlando, FL, Vol. 3, pp. 182–193.

Kearney, M., Cantoni, M. & Dower, P. M. 2011 Model predictive control for systems with scheduled load and its application to automated irrigation channels. *IEEE International Conference on Networking, Sensing and Control (ICNSC)*, Delft, The Netherlands, pp. 186–191.

Linke, H. 2005 Wasserbewirtschaftung von Binnenschifffahrtsgewässern auf Basis einer modellgestützten Vorhersage des Systemverhaltens. PhD Thesis, Ilmenau University of Technology.

Linke, H. 2007 Erfahrungen aus dem Wirkbetrieb der wasserwirtschaftlichen Optimierung fur das Kanalsystem Mittellandkanal/Elbe-Seitenkanal. Technical Report (unpublished). Ilmenau.

Litrico, X. & Georges, D. 1999 Robust continous-time and discrete-time flow control of a dam-river system. (I) Modelling. *Applied Mathematical Modelling* **23**, 809–827.

Negenborn, R. R., Sahin, A., Lukszo, Z., De Schutter, B. & Morari, M. 2009 A noniterative cascaded predictive control approach for control of irrigation canals. *Proc. of the IEEE Int. Conf. on Systems, Man, and Cybernetics*, San Antonio, TX, pp. 3552–3557.

Rao, C. V., Wright, S. J. & Rawlings, J. B. 1998 On the application of interior point methods to model predictive control. *Journal of Optimization Theory and Applications* **99** (3), 723–757.

Rawlings, J. B. & Mayne, D. Q. 2009 *Model Predictive Control: Theory and Design*. Nob Hill, Madison, WI.

Roe, P. L. 1981 Approximate Riemann solvers, parameter vectors, and difference schemes. *Journal of Computational Physics* **43**, 357–372.

Ruiz, C. & Ramirez, L. 1998 Predictive control in irrigation canal operation. *IEEE Int. Conference on Systems, Man & Cybernetics (SMC'98)*, San Diego, CA, pp. 3897–3901.

Sager, S. 2005 Numerical Methods for Mixed-integer Optimal Control Problems. PhD Thesis, Heidelberg University.

Sawadogo, S., Faye, R. M., Malaterre, P. O. & Mora-Camino, F. 1998 Decentralized predictive controller for delivery canals. *IEEE Int. Conference on Systems, Man & Cybernetics (SMC'98)*, San Diego, CA, pp. 3880–3884.

Schwanenberg, D., van Breukelen, A. & Hummel, S. 2011 Data assimilation for supporting optimum control in large-scale river networks. *IEEE International Conference on Networking, Sensing and Control (ICNSC)*, Delft, The Netherlands, pp. 98–103.

Setz, C., Heinrich, A., Rostalski, P., Papafotiou, G. & Morari, M. 2008 Application of model predictive control to a cascade of river power plants. 17th IFAC World Congress, Seoul, pp. 11978–11983.

Sohlberg, B. & Sernfält, M. 2002 Grey box modelling for river control. *Journal of Hydroinformatics* **4** (4), 265–280.

Thai, T. H. 2005 Numerical Methods for Parameter Estimation and Optimal Control of the Red River Network. PhD Thesis, Heidelberg University.

van der Merwe, R. & Wan, E. A. 2001 The square-root unscented Kalman filter for state and parameter estimation. *Proc. of the Int. Conf. on Acoustics, Speech, and Signal Processing (ICASSP)*, Salt Lake City, Utah, IEEE, Vol. 6. pp. 3461–3464.

Van Overloop, P.-J. 2006 Model Predictive Control on Open Water Systems. PhD Thesis, Delft University of Technology.

Van Overloop, P.-J., Negenborn, R. R., Weijs, S. V., Malda, W., Bruggers, M. R. & De Schutter, B. 2010 Linking water and energy objectives in lowland areas through the application of model predictive control. *IEEE Conference on Control Applications (CCA)*, Yokohama, pp. 1887–1891.

Wagenpfeil, J., Arnold, E. & Sawodny, O. 2010 Modeling and optimized water management of inland waterway systems. *IEEE Conference on Control Applications (CCA)*, Yokohama, pp. 1874–1880.

Wahlin, B. T. 2004 Performance of model predictive control on ASCE test canal 1. *Journal of Irrigation and Drainage Engineering* **130** (3), 227–238.

Weyer, E. 2001 System identification of an open water channel. *Control Engineering Practice* **9** (12), 1289–1299.

First received 31 October 2011; accepted in revised form 24 July 2012. Available online 18 December 2012